thank the UCLA Campus Computing Network for a grant of computing time and for use of computing equipment.

Registry No. $(C_6H_5)_3PAgCl$, 52495-09-7; $(C_6H_5)_3PAgBr$, 47107-31-3; $(C_6H_5)_3PAgI$, 61026-08-2; $(C_6H_5)_3PAgN_3$, 61062-63-3; $(C_6H_5)_3PAgNO_3$, 61026-18-4; $(C_6H_5)_3PAgCN\cdot 2CH_3CN$, 61026-09-3.

Supplementary Material Available: Table V, the calculated (idealized) positions and assigned isotropic thermal parameters of the hydrogen atoms, and Table VI, the observed and calculated structure factors (11 pages). Ordering information is given on any current masthead page.

References and Notes

(1) E. L. Muetterties and C. W. Alegranti, *J. Am. Chem. Soc.*, **94**, 6386 (1972).
(2) (a) M. R. Churchill and B. G. DeBoer, *Inorg. Chem.*, **14**, 2502 (1975); (b) B. K. Teo and J. C. Calabrese, *J. Am. Chem. Soc.*, **97**, 1256 (1975).
(3) D. H. Williams, R. S. Ward, and R. G. Cooks, *J, Am. Chem. Soc.*, **90**, 966 (1968).
(4) The background used in the mass spectral analysis of the peak at m/e 28 contained N_2 and CO in the ratio 10:1. Melting nitrato(triphenylphosphine)silver(I) in a tube attached to the spectrometer gave a 19% increase in N_2 and a 3.7-fold increase in CO. It is possible the increase in N_2 arose from atmospheric gas entrained in the crystals rather than by reduction of nitrate.
(5) J. D. McCullough, *Inorg. Chem.*, **12**, 2669 (1973).
(6) C. Knobler and J. D. McCullough, *Inorg. Chem.*, **11**, 3026 (1972).
(7) $R = \sum||F_o| - |F_c||/\sum|F_o|$; $w = [1/\sigma(F_o)]^2$.
(8) Supplementary material.
(9) "International Tables for X-Ray Crystallography", Vol. III, Kynoch Press, Birmingham, England, 1962.
(10) R. F. Stewart, E. R. Davidson, and W. T. Simpson, *J. Chem. Phys.*, **42**, 3175 (1965).
(11) C. C. Addison, N. Logan, and J. C. Wallwork, *Q. Rev., Chem. Soc.*, **25**, 289 (1971).
(12) M. K. Cooper and R. S. Nyholm, *J. Chem. Soc., Chem. Commun.*, 343 (1974).
(13) O. Ermer, H. Eser, and J. D. Dunitz, *Helv. Chim. Acta*, **54**, 2469 (1971), and references therein.
(14) D. J. Robinson and C. H. L. Kennard, *J. Chem. Soc. B*, 965 (1970).
(15) R. L. Bodner and A. I. Popov, *Inorg. Chem.*, **11**, 1410 (1972).
(16) J. H. Meiners, J. C. Clardy, and J. G. Verkade, *Inorg. Chem.*, **14**, 632 (1975).
(17) L. Pauling, "The Nature of the Chemical Bond", 3d ed, Cornell University Press, Ithaca, N.Y., 1960.
(18) J. Howatson and B. Morosin, *Cryst. Struct. Commun.*, **2**, 51 (1973).
(19) D. Coucouvanis, N. C. Baenziger, and S. M. Johnson, *Inorg. Chem.*, **13**, 1191 (1974).

Contribution from the Department of Inorganic Chemistry, University of Sydney, NSW 2006, Australia

Structure of Hexaaquairon(III) Nitrate Trihydrate. Comparison of Iron(II) and Iron(III) Bond Lengths in High-Spin Octahedral Environments

NEIL J. HAIR and JAMES K. BEATTIE*

Received July 14, 1976 AIC60504F

The structure of hexaaquairon(III) nitrate trihydrate, $[Fe(H_2O)_6](NO_3)_3\cdot 3H_2O$, has been determined from x-ray diffraction data collected by counter methods. The compound crystallizes in space group $P2_1/c$ (C_{2h}^5) with a = 13.989 (1) Å, b = 9.701 (1) Å, c = 11.029 (1) Å, β = 95.52 (1)°, Z = 4, ρ_{measd} = 1.81 (1) g cm^{-3}, and ρ_{calcd} = 1.80 g cm^{-3}. The intensities of 2209 reflections were measured with $I > 1.5\sigma(I)$. The structure was refined by full-matrix least-squares methods to a conventional R index (on F) of 0.042. The structure comprises two crystallographically distinct $Fe(H_2O)_6^{3+}$ octahedra, each possessing crystallographic ($\bar{1}$) symmetry, connected by a complex hydrogen-bonded network involving the nitrate anions and lattice water molecules. The mean Fe^{III}–O distance (1.986 (7) Å) is 0.14 Å shorter than the Fe^{II}–O distance in hexaaquairon(II) ions. This substantial difference in the iron–oxygen bond distances between $Fe(H_2O)_6^{3+}$ and $Fe(H_2O)_6^{2+}$ is interpreted using qualitative ligand field theory.

Introduction

There appears to be little structural information available for aquairon(III) species. A recent survey listed the *trans*-$Fe(H_2O)_4Cl_2^+$ structure but no data for penta- or hexaaquairon(III) complexes.[1] A structural analysis of an $Fe(H_2O)_6^{3+}$ salt is desirable, not only because of the general importance of this ion in transition metal chemistry but also for the specific analysis of the rates of electron-transfer reactions. The Hush–Marcus model of outer-sphere electron-transfer reactions has successfully accounted for the rate of electron exchange between $Fe(H_2O)_6^{3+}$ and $Fe(H_2O)_6^{2+}$, using an *estimated* difference of 0.16 Å in iron–oxygen bond distances between the two oxidation states.[2] However, recent crystallographic evidence[3] suggests that, in the absence of spin state changes, there is a much smaller difference in bond distances between oxidation states in octahedral complexes. This would lead to a negligible coordination sphere reorganization energy and the predicted rate would be much faster than the observed rate.

To resolve this conflict we have determined the crystal and molecular structure of $Fe(NO_3)_3\cdot 9H_2O$, following the report of its unit cell parameters.[4] A subsequent survey of the literature through 1973, accessed through BIDICS,[5] revealed mineralogical examples of aquairon(III) complexes, one of which contains an $Fe(H_2O)_6^{3+}$ species.[6] Its structure is consistent with the one reported here.

Experimental Section

Crystals of $[Fe(H_2O)_6](NO_3)_3\cdot 3H_2O$ can be recrystallized by slow evaporation from dilute nitric acid solutions. Difficulties were experienced in handling the crystals due to their hygroscopic character. Those selected for x-ray examination were first surface dried, coated with silicone grease, and then sealed in glass capillaries. Preliminary precession photography confirmed an earlier assignment of cell dimensions and space group.[4] The space group was uniquely determined as $P2_1/c$. The crystal density was measured as 1.81 (1) g cm^{-3} by flotation in a chloroform/bromoform mixture, the corresponding value calculated for Z = 4 being 1.80 g cm^{-3}. An oval plate of approximate dimensions 0.20 × 0.20 × 0.15 mm was selected for data collection and was mounted on an Enraf-Nonius four-circle CAD-4 diffractometer. Cell parameters were obtained by least-squares refinement of the 2θ values of 25 reflections measured with Mo $K\alpha_1$ radiation (λ 0.709 30 Å) in the range $53° < 2\theta < 56°$. The values obtained were a = 13.989 (1) Å, b = 9.701 (1) Å, c = 11.029 (1) Å, and β = 95.52 (1)°. Data were collected using Mo $K\alpha$ radiation from a graphite-crystal monochromator. The takeoff angle was 2.8° and the counter was positioned 17.3 cm from the crystal with an aperture 4.0 mm high by 2.0 mm wide. Profile analyses of a few low-angle reflections indicated that an ω–$^4/_3\theta$ scan method was most appropriate. Scan ranges (SR) were calculated from the formula SR = $M + W$ tan θ, where M is estimated from the mosaic spread of the crystal and W allows for increasing peak width due to $K\alpha_1$ and $K\alpha_2$ splitting. M and W were chosen as 1.5° and 0.35°, respectively. Each calculated scan range is extended on either side by 25% to accommodate the moving-background determinations (B_1 and B_2). The net intensity is I = PI − 2(B_1 + B_2), where PI is the peak intensity. The scan rate

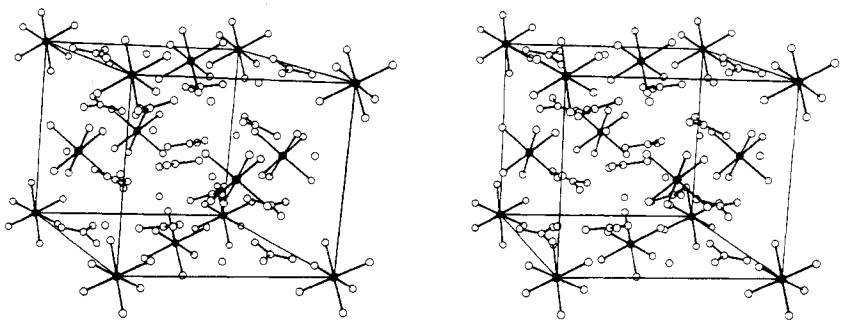

Figure 1. Stereoscopic view of the unit cell of $[Fe(H_2O)_6](NO_3)_3 \cdot 3H_2O$. The x axis points into the paper, the y axis is vertical, and the z axis is horizontal. The Fe atoms have been darkened and the H atoms omitted for clarity. The lattice waters are represented by open circles.

was optimized by a rapid prescan technique to obtain a $\sigma(I)/I$ ratio of 0.015 in the final scan, where $\sigma(I) = [PI + 4(B_1 + B_2)]^{1/2}$. The minimum and maximum scan rates used were 1.2 and 10°/min, respectively. A total of 3606 independent reflections were collected in the range $3° \leq 2\theta \leq 56°$.

Crystal movement was a severe problem during the data collection. This was overcome by a reorientation facility on the CAD-4, whereby the orientation matrix can be recalculated whenever the measured scattering vector for a reflection is found to deviate from its calculated position by more than a specified value (0.2° in this case). The intensities of three standard reflections, which were monitored every 3000 s of x-ray exposure, showed an overall decomposition effect of approximately 25%.

The data were corrected for Lorentz and polarization effects and also for decomposition effects. The latter correction was applied by a least-squares fitting of the measured intensity variation in consecutive standard groups to linear functions of the x-ray exposure time. The segments of data between standard groups were then rescaled to time zero using the correction factors obtained from the line-fitting technique. In view of the problems encountered with crystal movement and decomposition effects, two equivalent data sets ($\pm hk-l$ and $\pm h-kl$; total 494 reflections) were measured at different x-ray exposure times in order to assess the quality of the main data set after corrections had been applied. Comparison of equivalent $|F_o|$ measurements with their respective weighted mean values showed good correlation between data sets. An estimate of the goodness of fit (1.9%) was obtained from the index

$$[\sum_{\tilde{h}}\sum_{i} w_{\tilde{h}_i}(F_{\tilde{h}} - F_{\tilde{h}_i})^2 / \sum_{\tilde{h}}\sum_{i} w_{\tilde{h}_i} F_{\tilde{h}_i}^2]^{1/2}$$

where $\bar{F}_{\tilde{h}}$ is the weighted mean of the i observations of $F_{\tilde{h}_i}$ and $w_{\tilde{h}_i}$ is the statistical weight associated with each $F_{\tilde{h}_i}$ value. Absorption effects ($\mu = 11.4$ cm^{-1}) were difficult to assess owing to the awkward crystal shape. As a result of its hygroscopic character, the crystal appeared to adopt the shape of the capillary (radius 0.1 mm), and so absorption effects were estimated by considering a cylindrical correction with $\mu r = 0.1$.[7] Since, in the range $0° \leq 2\theta \leq 60°$, there is no variation in transmission factor ($A = 0.847$), absorption effects were ignored. The 2209 reflections with $I > 1.5\sigma(I)$ were used in the subsequent structure solution and refinement.

Analysis of the data with respect to parity group showed that reflections with either $(h + k)$ or $(k + l)$ or $(h + l)$ *even* were on average stronger than those with *odd* values for these combinations. This effect was most noticeable for the $(h + l)$ case. The pseudo-face-centered lattice, thus implied, was possible if the Fe^{3+} ions occupied two independent sets of special positions in $P2_1/c$, both of site symmetry $(\bar{1})$ [(a) 0, 0, 0; 0, $^1/_2$, $^1/_2$; (b) $^1/_2$, 0, $^1/_2$; $^1/_2$, $^1/_2$, 0]. A Patterson synthesis confirmed this assignment, both sets of Fe–O vectors being identified. After some initial problems of pseudo-symmetry, the complete structure was obtained by the heavy-atom method.

The structure was refined by full-matrix least-squares methods, the quantity minimized being $\sum w(|F_o| - |F_c|)^2$, where $|F_o|$ and $|F_c|$ are the observed and calculated structure amplitudes. The weights w were derived from an analytical expression $w = (a + b|F_o| + c|F_o|^2)^{-1}$, since analyses of $w(|F_o| - |F_c|)^2$, with respect to $|F_o|$, $(\sin\theta)/\lambda$, and Miller indices indicated that the weights derived from counting statistics did not adequately represent the inverse variances of the observations. The optimum values for the parameters a, b, and c were found to be 4.8158, −0.156 74, and 0.001 522 7, respectively. Values of the atomic scattering factors for Fe^{3+}, O, and N were taken from Cromer and Waber,[8] and those for H, from Stewart, Davidson, and Simpson.[9] Anomalous scattering terms were included for Fe.[10]

Table I. Final Fractional Coordinates[a]

Atom	x	y	z
Fe(1)	0	0	0
Fe(2)	$^1/_2$	0	$^1/_2$
O(1)	−0.070 14 (21)	0.088 17 (36)	−0.143 39 (27)
O(2)	0.096 40 (21)	0.150 69 (33)	0.004 39 (28)
O(3)	−0.076 12 (22)	0.108 86 (34)	0.108 97 (30)
O(4)	0.426 84 (21)	0.092 14 (37)	0.361 92 (27)
O(5)	0.599 21 (23)	0.147 22 (39)	0.499 49 (31)
O(6)	0.426 35 (23)	0.114 99 (36)	0.611 27 (28)
O(7)	0.115 01 (19)	0.217 16 (37)	0.290 58 (28)
O(8)	0.253 37 (18)	0.184 18 (32)	0.390 03 (24)
O(9)	0.236 99 (21)	0.165 61 (38)	0.193 45 (27)
O(10)	0.628 30 (21)	0.262 09 (41)	0.283 06 (29)
O(11)	0.773 86 (20)	0.259 26 (33)	0.367 23 (25)
O(12)	0.742 98 (22)	0.333 33 (39)	0.181 88 (29)
O(13)	−0.235 07 (19)	0.002 41 (38)	0.201 91 (24)
O(14)	−0.385 83 (19)	−0.046 88 (33)	0.163 08 (27)
O(15)	−0.301 28 (22)	0.014 01 (44)	0.019 53 (25)
O(16)	−0.034 95 (23)	0.379 24 (35)	0.127 43 (29)
O(17)	0.448 70 (24)	0.111 80 (40)	0.128 37 (29)
O(18)	0.144 30 (22)	0.474 69 (36)	0.048 82 (28)
N(1)	0.201 15 (23)	0.189 11 (37)	0.289 54 (30)
N(2)	0.714 96 (24)	0.285 77 (38)	0.277 31 (31)
N(3)	−0.307 15 (20)	−0.009 12 (40)	0.128 03 (26)

[a] Estimated standard deviations in the least significant figure(s) are given in parentheses in this and all subsequent tables.

Initial refinement, using isotropic temperature factors and positional parameters for nonhydrogen atoms, produced values of R $(=\sum||F_o| - |F_c||/\sum|F_o|)$ and R_w $(=(\sum w(|F_o| - |F_c|)^2/\sum w|F_o|^2)^{1/2})$ of 0.096 and 0.119, respectively. Introduction of anisotropic thermal parameters reduced R and R_w to 0.056 and 0.071. A difference Fourier map was then calculated, revealing the positions of the 18 hydrogen atoms. Since there was no reason to suppose a particular orientation for each water molecule, the observed hydrogen atom positions were allowed to vary in the final refinement cycles. Each hydrogen atom was assigned a fixed isotropic thermal parameter which corresponded to the last isotropic value of its attached oxygen atom. This introduction of 54 extra parameters for the 18 hydrogen atoms was significant at a >99% confidence level.[11] Refinement was terminated when the parameter shifts were less than 0.2σ. The final values for R and R_w were 0.042 and 0.035. The standard deviation of an observation of unit weight was 0.98, based on the 256 variables and 2209 observations. A final difference map showed no unusual features. A structure factor calculation was carried out including the 1397 reflections with $I < 1.5\sigma(I)$ which were omitted from the refinement. R and R_w were 0.099 and 0.058 respectively. A listing of $|F_o|$ and $|F_c|$ values is available (supplementary material). The final nonhydrogen atomic parameters with esd's are listed in Tables I and II, while those for the hydrogen atoms are listed in Table III. Figures 1 and 2 were drawn using Johnson's ORTEP2 thermal ellipsoid plotting program.

Description of Structure

The structure of $[Fe(H_2O)_6](NO_3)_3 \cdot 3H_2O$ contains two independent $Fe(H_2O)_6^{3+}$ ions, both of which exhibit crystallographic $(\bar{1})$ symmetry. The spatial arrangements of these

Table II. Anisotropic Thermal Parameters, Å²

Atom	U_{11}[a]	U_{22}	U_{33}	U_{12}	U_{13}	U_{23}
Fe(1)	1.54 (3)	2.16 (4)	1.83 (4)	−0.12 (4)	0.26 (3)	0.10 (4)
Fe(2)	1.67 (4)	2.97 (5)	1.60 (4)	0.04 (4)	0.24 (3)	0.28 (4)
O(1)	2.66 (16)	4.34 (21)	2.15 (15)	0.98 (14)	0.12 (13)	0.55 (15)
O(2)	2.56 (15)	3.32 (19)	2.30 (16)	−0.97 (14)	0.06 (15)	0.13 (15)
O(3)	2.67 (16)	2.77 (18)	4.03 (18)	−0.21 (15)	1.10 (13)	−0.85 (16)
O(4)	2.57 (15)	4.94 (22)	2.15 (15)	1.00 (15)	0.47 (13)	0.68 (16)
O(5)	3.03 (17)	5.27 (24)	2.82 (18)	−1.65 (16)	−0.10 (13)	0.93 (17)
O(6)	4.05 (18)	3.81 (20)	2.63 (16)	0.46 (17)	1.39 (13)	0.02 (14)
O(7)	1.87 (13)	6.57 (24)	3.96 (17)	0.84 (14)	−0.04 (11)	−1.23 (17)
O(8)	2.44 (13)	5.07 (19)	2.45 (13)	0.44 (13)	−0.18 (11)	−0.14 (13)
O(9)	2.89 (16)	6.89 (24)	2.42 (16)	0.54 (17)	0.39 (13)	−0.99 (17)
O(10)	2.54 (15)	7.31 (25)	4.48 (19)	−1.14 (17)	0.36 (14)	1.16 (18)
O(11)	3.52 (15)	4.54 (18)	2.71 (14)	−0.78 (14)	−0.61 (12)	0.59 (14)
O(12)	3.14 (16)	6.47 (23)	3.26 (18)	−0.61 (17)	0.44 (14)	1.53 (18)
O(13)	3.63 (14)	5.21 (18)	3.83 (14)	−0.24 (18)	−0.12 (11)	0.31 (19)
O(14)	3.02 (14)	5.65 (21)	4.86 (18)	−0.34 (14)	1.60 (13)	0.52 (15)
O(15)	4.97 (17)	7.95 (26)	3.30 (14)	−1.46 (21)	0.83 (13)	1.61 (19)
O(16)	3.11 (16)	3.47 (19)	3.24 (17)	0.25 (14)	0.73 (13)	0.19 (14)
O(17)	2.90 (16)	5.64 (24)	2.86 (17)	−0.05 (16)	0.37 (13)	−0.28 (16)
O(18)	4.16 (17)	4.70 (24)	3.53 (16)	−0.39 (15)	−0.09 (13)	−0.97 (15)
N(1)	2.52 (17)	3.03 (19)	2.58 (17)	0.25 (15)	0.33 (14)	−0.31 (15)
N(2)	2.55 (17)	3.18 (20)	2.97 (19)	−0.46 (15)	0.28 (15)	0.03 (18)
N(3)	2.74 (14)	3.10 (17)	3.04 (15)	0.01 (18)	0.29 (12)	−0.23 (18)

[a] The form of the anisotropic thermal ellipsoid is $\exp[-2\pi^2(U_{11}h^2a^{*2} + U_{22}k^2b^{*2} + U_{33}l^2c^{*2} + 2U_{12}hka^*b^* + 2U_{13}hla^*c^* + 2U_{23}klb^*c^*]$. The values given in the table are $U_{ij} \times 10^2$.

Table III. Hydrogen Atom Fractional Coordinates and Isotropic Thermal Parameters

Atom[a]	x	y	z	U_{iso},[b] Å²
H(11)	−0.0569 (31)	0.0869 (48)	−0.2174 (43)	0.0299
H(12)	−0.1107 (33)	0.1312 (50)	−0.1309 (44)	0.0299
H(21)	0.1034 (30)	0.2063 (45)	−0.0593 (40)	0.0272
H(22)	0.1378 (32)	0.1585 (50)	0.0605 (42)	0.0272
H(31)	−0.0650 (33)	0.1886 (52)	0.1206 (42)	0.0308
H(32)	−0.1310 (32)	0.0765 (45)	0.1263 (38)	0.0308
H(41)	0.4354 (31)	0.0892 (47)	0.2871 (43)	0.0290
H(42)	0.3755 (34)	0.1288 (47)	0.3688 (41)	0.0290
H(51)	0.6114 (33)	0.1793 (50)	0.4398 (45)	0.0337
H(52)	0.6393 (35)	0.1512 (53)	0.5525 (46)	0.0337
H(61)	0.4313 (33)	0.2050 (52)	0.6044 (43)	0.0325
H(62)	0.4007 (30)	0.0752 (46)	0.6766 (40)	0.0325
H(161)	−0.0658 (33)	0.4197 (50)	0.0744 (43)	0.0322
H(162)	0.0185 (34)	0.3969 (49)	0.1150 (41)	0.0322
H(171)	0.4123 (34)	0.0752 (52)	0.0790 (43)	0.0355
H(172)	0.4967 (34)	0.0723 (51)	0.1172 (42)	0.0355
H(181)	0.1767 (34)	0.4177 (53)	0.0183 (44)	0.0393
H(182)	0.1668 (34)	0.5173 (56)	0.1026 (42)	0.0393

[a] Hydrogen atoms are numbered according to their attached oxygen atoms. [b] Hydrogen atom isotropic thermal parameters were set equal to the last isotropic values of their attached oxygen atoms.

Table IV. Bond Distances (Å) and Angles (deg)

	(a) Octahedron 1		
Fe(1)-O(1)	1.974 (3)	O(1)-Fe(1)-O(2)	89.1 (1)
Fe(1)-O(2)	1.986 (3)	O(1)-Fe(1)-O(3)	90.0 (1)
Fe(1)-O(3)	1.985 (3)	O(2)-Fe(1)-O(3)	89.8 (1)
	(b) Octahedron 2		
Fe(2)-O(4)	1.966 (3)	O(4)-Fe(2)-O(5)	89.0 (1)
Fe(2)-O(5)	1.992 (3)	O(4)-Fe(2)-O(6)	87.8 (1)
Fe(2)-O(6)	2.014 (3)	O(5)-Fe(2)-O(6)	90.1 (1)
	(c) Nitrate 1		
N(1)-O(7)	1.237 (4)	O(7)-N(1)-O(8)	118.7 (3)
N(1)-O(8)	1.268 (4)	O(7)-N(1)-O(9)	121.6 (3)
N(1)-O(9)	1.237 (4)	O(8)-N(1)-O(9)	119.7 (3)
	(d) Nitrate 2		
N(2)-O(10)	1.242 (4)	O(10)-N(2)-O(11)	119.5 (3)
N(2)-O(11)	1.253 (4)	O(10)-N(2)-O(12)	120.0 (3)
N(2)-O(12)	1.247 (5)	O(11)-N(2)-O(12)	120.5 (3)
	(e) Nitrate 3		
N(3)-O(13)	1.239 (4)	O(13)-N(3)-O(14)	120.4 (3)
N(3)-O(14)	1.256 (4)	O(13)-N(3)-O(15)	119.9 (3)
N(3)-O(15)	1.228 (4)	O(14)-N(3)-O(15)	119.7 (3)

ions in the lattice (see Figure 1) show that an exact B-face centering exists with respect to the FeO_6 units but that A-face and C-face centering are present only with respect to the central Fe(III) atoms. Such an arrangement confirms the pseudo face centerings which were implied by the initial analysis of the x-ray data. The independent $Fe(H_2O)_6^{3+}$ ions are linked by hydrogen bonding to three nitrate groups and three lattice water molecules. The packing of these species in the unit cell is shown in Figure 1. Intramolecular bond distances and angles are listed in Table IV. Figure 2 shows the "asymmetric unit" of the cell and illustrates the overall similarities of the two independent $Fe(H_2O)_6^{3+}$ octahedra and also the similarities of the hydrogen-bonded networks in which each is involved (see also Table V).

Where the hydrogen atoms of lattice water molecules are involved in hydrogen bonds, the bonds are longer than those which involve water molecules coordinated to Fe(III) (see Table V). The other essential components of the hydrogen-bonded network are the planar nitrate ions, in which each oxygen atom acts as an acceptor atom for at least one hydrogen bond. Three oxygen atoms (O(8) of nitrate 1; O(13) and O(14) of nitrate 3) act as acceptor atoms for one short hydrogen bond to a coordinated water molecule and also one longer bond to a lattice water molecule (see Figure 2 and Table V). Within nitrate 1 the N–O(8) bond is significantly lengthened. There is no correlation, however, between the number of hydrogen bonds and the N–O bond lengths in nitrate 3.

Comparison of the two distinct types of water molecules in the structure indicates the following points. (a) Coordinated water molecules adopt a trigonal configuration with the Fe–O bond directed along the bisectrix of the oxygen atom lone pairs. The mean bond angle at these coordinated oxygen atoms is 119 (1)°. (b) Lattice water molecules, which are involved only in the formation of hydrogen bonds, adopt a tetrahedral configuration with two hydrogen bonds in the lone-pair directions. The mean bond angle at these oxygen atoms, including angles derived from hydrogen-bonded interactions, is 109 (2)°. These and other types of coordination have been summarized in a recent survey of the geometry and envi-

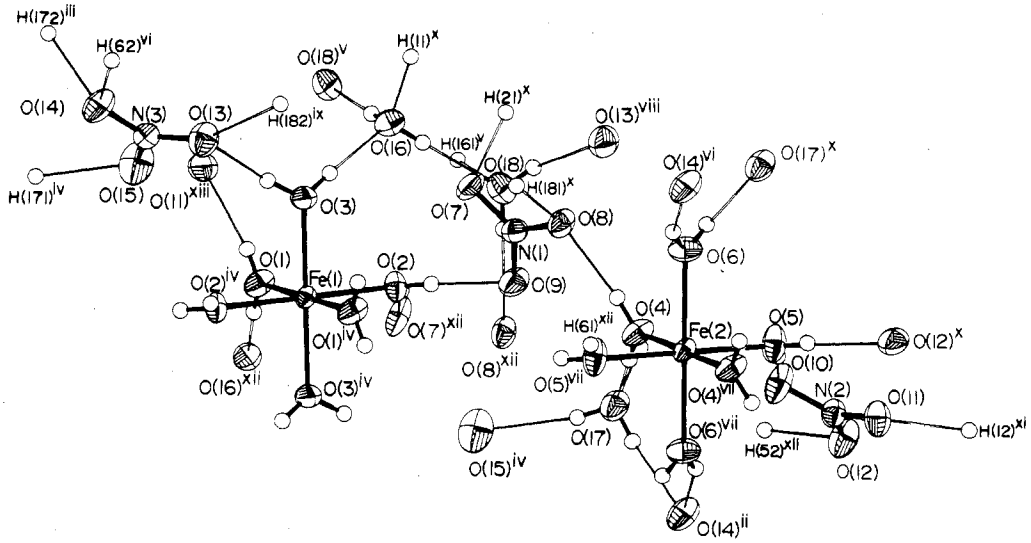

Figure 2. Perspective view of the asymmetric unit, illustrating the hydrogen-bonded network. Non-H atoms are drawn with 50% probability ellipsoids, and the H atoms are represented by circles of radius 0.1 Å. Covalent bonds and hydrogen bonds are represented by thick and thin bonds, respectively. Unlabeled H atoms are numbered according to their attached O atom. Symmetry codes are given in Table V. If a superscript is omitted, it is assumed to be i.

Table V. Distances and Angles Pertinent to the Hydrogen-Bonded Interactions D-H···A[a]

D-H···A[b]	D-H, Å	H···A, Å	D···A, Å	D-H···A, deg
O(1)-H(11)···O(16)^{xii}	0.85	1.80	2.640	168
O(1)-H(12)···O(11)^{xiii}	0.73	1.93	2.649	168
O(2)-H(21)···O(7)^{xii}	0.90	1.84	2.719	167
O(2)-H(22)···O(9)^{i}	0.81	1.92	2.729	177
O(3)-H(31)···O(16)^{i}	0.80	1.90	2.689	173
O(3)-H(32)···O(13)^{i}	0.87	1.89	2.739	166
O(4)-H(41)···O(17)^{i}	0.85	1.79	2.630	171
O(4)-H(42)···O(8)^{i}	0.81	1.83	2.632	171
O(5)-H(51)···O(10)^{i}	0.76	1.94	2.700	174
O(5)-H(52)···O(12)^{x}	0.77	1.94	2.711	178
O(6)-H(61)···O(17)^{x}	0.88	1.81	2.673	167
O(6)-H(62)···O(14)^{vi}	0.92	1.82	2.688	156
O(16)-H(161)···O(18)^{v}	0.80	1.95	2.749	177
O(16)-H(162)···O(18)^{i}	0.79	2.11	2.884	166
O(17)-H(171)···O(15)^{iv}	0.79	2.00	2.785	168
O(17)-H(172)···O(14)^{ii}	0.79	2.03	2.776	156
O(18)-H(181)···O(8)^{xii}	0.81	2.10	2.878	161
O(18)-H(182)···O(13)^{viii}	0.76	2.28	2.928	143

[a] Average esd's in the tabulated values: D-H, 0.05 Å; H···A, 0.05 Å; D···A, 0.004 Å; D-H···A, 5°. Mean O-H = 0.82 (2) Å. [b] Symmetry codes for atom A are listed as follows (also included are symmetry codes relating to the hydrogen-bonding scheme in Figure 2): (i) x, y, z; (ii) $1+x, y, z$; (iii) $-1+x, y, z$; (iv) $-x, -y, -z$; (v) $-x, 1-y, -z$; (vi) $-x, -y, 1-z$; (vii) $1-x, -y, 1-z$; (viii) $-x, {}^1/_2+y, {}^1/_2-z$; (ix) $-x, -{}^1/_2+y, {}^1/_2-z$; (x) $x, {}^1/_2-y, {}^1/_2+z$; (xi) $1+x, {}^1/_2-y, {}^1/_2+z$; (xii) $x, {}^1/_2-y, -{}^1/_2+z$; (xiii) $-1+x, {}^1/_2-y, -{}^1/_2+z$.

ronment of water molecules in crystalline hydrates.[12] Types (a) and (b) in the present structure have been classified as class 1M and class 2E interactions, respectively.

The independent $Fe(H_2O)_6^{3+}$ ions possess almost regular octahedral geometry. The mean Fe^{III}–O bond length, averaged over the independent octahedra, is 1.986 (7) Å where the deviation in the mean value is an unbiased estimate. It is apparent that the Fe(2)–O(6) bond (2.014 (3) Å) lies significantly outside the range described by the mean value. We noted earlier that the hydrogen-bonding patterns around both octahedra were almost identical. However, a closer examination reveals that, in order to maximize hydrogen-bonded interactions with the appropriate acceptor atoms, the O(6) water molecule is rotated about the Fe(2)–O(6) bond by 37° with respect to the O(5)–Fe(2)–O(6) plane. The mean rotation of the molecular plane for the other five-coordinated waters is 13 (3)°. It is feasible that this extra rotation to accommodate hydrogen-bonded interactions in the O(6) case has introduced additional antibonding character into the Fe(2)–O(6) bond, thus lengthening the bond. However, we find that a general correlation between Fe^{III}–O bond length and rotation of the water molecular plane is not statistically significant.

Discussion

The iron(III)–oxygen distance of 1.986 (7) Å found in this study and the identical value of 1.98 (2) Å found in the mineral paracoquimbite[6] represent the shortest Fe^{III}–O distances yet determined for coordinated water molecules. These are the only determinations of an $Fe(H_2O)_6^{3+}$ octahedron known to us. The introduction of other ligands into the coordination sphere results in the lengthening of the iron–oxygen distances of the remaining water molecules, reaching a maximum of 2.11 Å for the seven-coordinate $[Fe(EDTA)H_2O]^-$ anion[13,14] (Table VI). With coordinated sulfate anions the Fe^{III}–O distance for the water molecules is in the range 1.99–2.03 Å,[15-19] but with chloride ions in the coordination sphere the Fe^{III}–O distance is 2.07–2.08 Å.[20-22]

A comparison of the metal–ligand distances between the hexaaquairon(II) and -iron(III) complexes is the critical purpose of this work. There have been at least three determinations of structures containing the $Fe(H_2O)_6^{2+}$ species. Although the range of bond distances within each structure is somewhat wider than for Fe(III), the mean values are in good agreement: 2.12 Å in $FeSO_4 \cdot 7H_2O$,[23] 2.13 Å in $(NH_4)_2Fe(SO_4)_2 \cdot 6H_2O$,[24] and 2.15 Å in $Fe(H_2O)_6SiF_6$.[25] Using an average of 2.13 Å for iron(II), we find that the difference in metal–ligand bond distances between the two oxidation states is thus about 0.14 Å.

This large difference approaches that of 0.18 Å found between $Co(NH_3)_6^{2+}$ and $Co(NH_3)_6^{3+}$,[26,27] which has been ascribed to the change in electron spin state between low-spin cobalt(III) and high-spin cobalt(II). However, both hexaaquairon complexes are high spin. We conclude that a change in spin state is not a prerequisite for substantial differences in metal–ligand bond lengths between different oxidation states of octahedral metal complexes.

These differences in metal–ligand distances are consistent, however, with a qualitative description of bonding in metal

Table VI. Iron(III)–Oxygen Distances of Coordinated Water

Av dist, Å	Coordination sphere	Compd	Ref
1.98	$Fe(H_2O)_6$	Paracoquimbite, $Fe_2(SO_4)_3 \cdot 9H_2O$	6
1.99	$Fe(H_2O)_6$	$Fe(NO_3)_3 \cdot 9H_2O$	This work
2.00	*fac*-$Fe(H_2O)_3(OSO_3)_3$	Paracoquimbite, $Fe_2(SO_4)_3 \cdot 9H_2O$	6
1.99			
2.00	*trans*-$Fe(H_2O)_2(OSO_3)_4$	$NH_4Fe(SO_4)_2 \cdot 3H_2O$	15
2.01	$Fe(H_2O)_5OSO_3$	Quenstedite, $[Fe_2(H_2O)_9(SO_4)_3] \cdot 2H_2O$	16
2.01	*mer*-$Fe(H_2O)_3(OSO_3)_3$	Kornelite, $[Fe_2(H_2O)_6(SO_4)_3] \cdot 1.25H_2O$	17
2.01	*fac*-$Fe(H_2O)_3(OSO_3)_3$	Coquimbite, $Fe_{2-x}Al_x(SO_4)_3 \cdot 9H_2O$	18
2.02	*cis*-$Fe(H_2O)_4(OSO_3)_2$	Quenstedite, $[Fe_2(H_2O)_9(SO_4)_3] \cdot 2H_2O$	16
2.03	*cis*-$Fe(H_2O)_4(OSO_3)_2$	Roemerite, $Fe_3(SO_4)_4 \cdot 14H_2O$	19
2.07	*trans*-$Fe(H_2O)_4Cl_2$	$[Fe(H_2O)_4Cl_2]Cl$	20
2.07	$Fe(HEDTA)H_2O$	$Fe(HEDTA)H_2O$	14
2.08	*trans*-$Fe(H_2O)_4Cl_2$	$[Fe(H_2O)_4Cl_2]SbCl_6 \cdot 4H_2O$	21
2.08	$Fe(H_2O)Cl_5$	$(NH_4)_2[Fe(H_2O)Cl_5]$	22
2.09	$Fe(DCTA)H_2O$	$Ca[Fe(DCTA)H_2O] \cdot 8H_2O$	14
2.11	$Fe(EDTA)H_2O$	$Rb[Fe(EDTA)H_2O] \cdot H_2O$	13
2.11	$Fe(EDTA)H_2O$	$Li[Fe(EDTA)H_2O] \cdot H_2O$	13

Table VII. Comparison of Metal–Ligand Bond Distances (Å) between M(II) and M(III) Oxidation States

	r(M–L)	Δr(M–L)	Ref
$Co(NH_3)_6^{2+}$	2.114	Co–N 0.18	26
$Co(NH_3)_6^{3+}$	1.936		27
$Fe(H_2O)_6^{2+}$	2.13 (av)	Fe–O 0.14	23–25
$Fe(H_2O)_6^{3+}$	1.99		This work, 6
$FeCl_4^{2-}$	2.292	Fe–Cl 0.11	2
$FeCl_4^-$	2.185		34
trans-$Cr(H_2O)_4Cl_2$	2.078 (O)		32
	2.758 (Cl)	Cr–O 0.07	
trans-$Cr(H_2O)_4Cl_2^+$	2.005 (O)	Cr–Cl 0.47	31
	2.289 (Cl)		
trans-$Fe(H_2O)_4Cl_2$	2.10 (O) (av)		33
	2.52 (Cl) (av)	Fe–O 0.03	
trans-$Fe(H_2O)_4Cl_2^+$	2.07 (O)	Fe–Cl 0.22	20, 21
	2.30 (Cl)		
$Ru(NH_3)_6^{2+}$	2.144	Ru–N 0.04	30
$Ru(NH_3)_6^{3+}$	2.104		
$Fe(phen)_3^{2+}$	1.97	Fe–N 0.00	28
$Fe(phen)_3^{2+}$	1.97		29

complexes using simple molecular orbital theory. Table VII lists metal complexes in which an identical coordination sphere has been determined crystallographically in both the II and III oxidation states. The smallest differences occur for the $Fe(phen)_3^{3+}$–$Fe(phen)_3^{2+}$ pair (0.00 Å)[28,29] and the $Ru(NH_3)_6^{3+}$–$Ru(NH_3)_6^{2+}$ pair (0.04 Å).[30] The electron configurations are low-spin $(t_{2g})^5$ and low-spin $(t_{2g})^6$ for the III and II oxidation states, respectively. The difference is one "nonbonding" t_{2g} electron. The identical bond lengths for the phenanthroline complexes suggest that the expected lengthening of the bond in the II oxidation state due to electrostatic effects is just compensated by increased π back-bonding, so that the t_{2g} electrons become slightly bonding in this state.

The largest difference occurs for the $Co(NH_3)_6^{3+}$–$Co(NH_3)_6^{2+}$ pair (0.18 Å) with the electron configurations $(t_{2g})^6$ and $(t_{2g})^5(e_g^*)^2$. Here the two antibonding electrons in the cobalt(II) complex result in a substantial lengthening of the metal–ligand bonds.

From these examples it was reasonable to predict[3] that the difference would be small between the electron configurations high-spin d^5, $(t_{2g})^3(e_g^*)^2$, and high-spin d^6, $(t_{2g})^4(e_g^*)^2$, which occur in the hexaaquairon complexes. The difference is again a single t_{2g} electron. This argument, however, fails to recognize two points. First, in weak-field, high-spin complexes the t_{2g} electrons are antibonding with respect to the π electrons of the ligands. Thus the introduction of a formally σ-nonbonding t_{2g} electron on the reduction of $Fe(H_2O)_6^{3+}$ to $Fe(H_2O)_6^{2+}$ results in an increase in bond length due to π-antibonding interaction with the lone-pair electrons on the oxygen atom.

Second, the one-electron description of electronic structure is less appropriate for weak-field than for strong-field complexes. Even in the absence of π-bonding effects, the weaker ligand field in the lower oxidation state results in additional antibonding character. These effects mean that *bond length differences between oxidation states are greater for high-spin than for low-spin octahedral complexes.*

Similar arguments can be used to account for the other differences listed in Table VII. In the one-electron model the difference between the $(t_{2g})^3$ description of $Cr(H_2O)_4Cl_2^+$ [31] and the $(t_{2g})^3(e_g^*)^1$ description of $Cr(H_2O)_4Cl_2$ [32] is one antibonding e_g^* electron in the d_{z^2} orbital, resulting in an increase in the Cr–Cl distance of 0.47 Å. The difference between the $(t_{2g})^3(e_g^*)^2$ description of $Fe(H_2O)_4Cl_2^+$ [20] and the $(t_{2g})^4(e_g^*)^2$ description of $Fe(H_2O)_4Cl_2$ [33] is not one nonbonding t_{2g} electron, however, but the addition of considerable antibonding character, again directed principally along the weaker field z axis, resulting in an increase in the Fe–Cl distance of 0.22 Å. Finally, the difference of 0.11 Å between the tetrachloroferrate structures[3,34] reflects the antibonding nature of the e electron introduced on reduction of iron(III) to iron(II) in a tetrahedral environment.

Calculations based on the Hush–Marcus model for the rate of electron transfer between $Fe(H_2O)_6^{2+}$ and $Fe(H_2O)_6^{3+}$ have been made using Fe–O distances of 2.05 and 2.21 Å, respectively.[2] Although these are now known to be in error, the difference between the two oxidation states remains almost the same. Since it is the difference and not the absolute values which is the critical quantity in assessing the inner coordination sphere barrier to electron transfer, these calculations remain valid. The relatively slow rate of electron exchange between these hexaaqua ions is due to a considerable inner coordination sphere reorganization energy barrier resulting from the large difference in bond lengths between the two oxidation states.

We conclude that a simple ligand field model qualitatively accounts for the observed differences in bond distances but that the nature of the ligands must be considered in addition to the formal d-electron configuration. Our results are in good agreement with the ionic radii tabulated by Shannon and Prewitt[35] for the oxides and fluorides of the transition metals. These radii are appropriate for such antibonding ligands but would probably be inappropriate for strong-field ligands such as NH_3, phen, or CN^-.

Acknowledgment. We thank Professor H. C. Freeman for the use of the diffraction laboratory, Dr. J. M. Guss for helpful discussions, and Dr. S. Morup for useful correspondence. This work was supported by a University of Sydney research grant and by the Australian Research Grants Committee.

Note Added in Proof. An important article by B. I. Swanson, S. I. Hamburg, and R. R. Ryan, [*Inorg. Chem.*, **13**,

1685 (1974)] establishes a *decrease* in Fe–C distance of 0.026 (8) Å from $Fe(CN)_6^{3-}$ to $Fe(CN)_6^{4-}$, ascribed by these authors to an increase in π bonding in the Fe(II) state. This should be the final entry in Table VII and is consistent with the interpretation presented here.

Registry No. $[Fe(H_2O)_6](NO_3)_3 \cdot 3H_2O$, 60803-54-5.

Supplementary Material Available: Listing of observed and calculated structure factor amplitudes (22 pages). Ordering information is given on any current masthead page.

References and Notes

(1) S. A. Cotton, *Coord. Chem. Rev.*, **8**, 185 (1972).
(2) F. Basolo and R. G. Pearson, "Mechanisms of Inorganic Reactions", 1st ed, Wiley, New York, N.Y., pp 48, 307; N. S. Hush, *Trans. Faraday Soc.*, **57**, 557 (1961); N. Sutin, *Annu. Rev. Nucl. Sci.*, **12**, 285 (1962).
(3) J. W. Lauher and J. A. Ibers, *Inorg. Chem.*, **14**, 348 (1975).
(4) J. Villadsen, private communication, quoted by S. Morup and N. Thrane, *Chem. Phys. Lett.*, **21**, 363 (1973).
(5) I. D. Brown, Ed., "Bond Index to the Determinations of Inorganic Crystal Structures", Institute for Materials Research, McMaster University, Hamilton, Ontario, Canada.
(6) P. D. Robinson and J. H. Fang, *Am. Mineral.*, **56**, 1567 (1971).
(7) "International Tables for X-Ray Crystallography", Vol. II, Kynoch Press, Birmingham, England, 1972.
(8) D. T. Cromer and J. T. Waber, *Acta Crystallogr.*, **18**, 104 (1965).
(9) R. F. Stewart, E. R. Davidson, and W. T. Simpson, *J. Chem. Phys.*, **42**, 3175 (1965).
(10) D. T. Cromer, *Acta Crystallogr.*, **18**, 17 (1965).
(11) W. C. Hamilton, *Acta Crystallogr.*, **18**, 502 (1965).
(12) G. Ferraris and M. Franchini-Angela, *Acta Crystallogr., Sect. B*, **28**, 3572 (1972).
(13) M. D. Lind, M. J. Hamor, T. A. Hamor, and J. L. Hoard, *Inorg. Chem.*, **3**, 34 (1964).
(14) C. H. L. Kennard, *Inorg. Chim. Acta*, **1**, 347 (1968); G. H. Cohen and J. L. Hoard, *J. Am. Chem. Soc.*, **88**, 3228 (1966).
(15) K. J. Palmer, R. Y. Wong, and K. S. Lee, *Acta Crystallogr.*, **28**, 236 *Sect. B*, (1972).
(16) J. N. Thomas, P. D. Robinson, and J. H. Fang, *Am. Mineral.*, **59**, 582 (1974).
(17) P. D. Robinson and J. H. Fang, *Am. Mineral.*, **58**, 535 (1973).
(18) J. H. Fang and P. D. Robinson, *Am. Mineral.*, **55**, 1534 (1970).
(19) L. Fanfani, A. Nunzi, and P. F. Zanazzi, *Am. Mineral.*, **55**, 78 (1970).
(20) M. D. Lind, *J. Chem. Phys.*, **47**, 990 (1967).
(21) A. Ferrari, L. Cavalca, and M. E. Tani, *Gazz. Chim. Ital.*, **87**, 22 (1957).
(22) I. Lindqvist, *Ark. Kemi, Mineral. Geol.*, **24**, 1 (1947).
(23) W. H. Bauer, *Acta Crystallogr.*, **17**, 1167 (1964).
(24) H. Montgomery, R. V. Chastain, J. J. Natt, A. M. Witowska, and E. C. Lingafelter, *Acta Crystallogr.*, **22**, 775 (1967).
(25) W. C. Hamilton, *Acta Crystallogr.*, **15**, 353 (1962).
(26) T. Barnet, B. M. Craven, H. C. Freeman, N. E. Kime, and J. A. Ibers, *Chem. Commun.*, 307 (1966).
(27) N. E. Kime and J. A. Ibers, *Acta Crystallogr., Sect. B*, **25**, 168 (1969).
(28) A. Zalkin, D. H. Templeton, and T. Ueki, *Inorg. Chem.*, **12**, 1641 (1973).
(29) J. Baker, L. M. Engelhardt, B. N. Figgis, and A. H. White, *J. Chem. Soc., Dalton Trans.*, 530 (1975).
(30) H. C. Stynes and J. A. Ibers, *Inorg. Chem.*, **10**, 2304 (1971).
(31) I. G. Dance and H. C. Freeman, *Inorg. Chem.*, **4**, 1555 (1965).
(32) H. G. von Schnering and B.-H. Brand, *Z. Anorg. Allg. Chem.*, **402**, 159 (1973).
(33) J. Munier-Piret and M. Van Meerssche, *Acta Crystallogr., Sect. B*, **27**, 2329 (1971); J. J. Verbist, W. C. Hamilton, T. F. Koetzle, and M. S. Lehmann, *J. Chem. Phys.*, **56**, 3257 (1972).
(34) T. J. Kistenmacher and G. D. Stucky, *Inorg. Chem.*, **7**, 2150 (1968).
(35) R. D. Shannon and C. T. Prewitt, *Acta Crystallogr., Sect. B*, **25**, 925 (1969).

Contribution from the Laboratoire de Chimie Minerale, Faculte des Sciences, Universite de Reims, Reims, France

Crystal Structure and Spectral Properties of Sodium Dicyanocuprate(I) Dihydrate. A Planar Polymeric Three-Coordinated Copper(I) Anion

CHARLES KAPPENSTEIN and RENÉ P. HUGEL*

Received July 26, 1976 AIC60530D

The structure of sodium dicyanocuprate(I) dihydrate, $NaCu(CN)_2 \cdot 2H_2O$, has been determined crystallographically. The space group is $P2_1/c$ with $a = 3.598$ (3) Å, $b = 19.655$ (4) Å, $c = 8.515$ (5) Å, $\beta = 103.35$ (5)°, $Z = 4$, $V = 585.9$ Å^3, and a density of 1.97 g/cm^3. Based on 714 unique Weissenberg reflections, the structure was refined by full-matrix least-squares techniques to give $R = 0.058$ and $R_w = 0.064$. The structure is characterized by the existence of a polymeric $[Cu(CN)_2^-]_\infty$ chain having the symmetry of the glide plane c, with copper atoms in a trigonal-planar coordination. On each copper are fixed one terminal cyano group, Cu–C = 1.902 (7) Å, and two bridging groups, Cu–C = 1.904 (9) Å and Cu–N = 1.992 (8) Å. The sodium atom has an octahedral cis geometry formed by three oxygens and three nitrogens from terminal cyano groups. Two different types of water molecules are present. The Raman and infrared spectra as well as the reflectance spectrum are given.

Introduction

The cyanocuprate(I) ions $Cu(CN)_2^-$, $Cu(CN)_3^{2-}$, and $Cu(CN)_4^{3-}$ exist as such in aqueous solution,[1] but only the geometrical structure of the last anion is known in the potassium compound $K_3Cu(CN)_4$[2] where it is tetrahedral. The main characteristic of the other known cyanocuprates is the existence of polymeric anions containing bridging cyano groups. The coordination number around copper(I) is 3 (as in $KCu(CN)_2$[3]) or 4 (as in the mixed-valence complex $[Cu^I(CN)_2]_2[Cu^{II}(en)_2H_2O]$[4]). However very few data are available on the sodium salts of cyanocuprates and only ref 5 points out the two salts $NaCu(CN)_2 \cdot 2H_2O$ and $Na_2Cu(CN)_3 \cdot 3H_2O$ but without any structural information; on the other hand in the case of potassium salts a compound with a ratio CN:Cu = 3 is unknown[6] and the complex $KCu(CN)_2$ with a ratio CN:Cu = 2 is polymeric. Therefore it was interesting to investigate these two sodium salts and we report here the preparation, structure, and spectral properties of sodium dicyanocuprate(I) dihydrate. We hoped to find the monomeric anion $Cu(CN)_2^-$ on the basis of the following considerations: (1) It is a hydrated salt and the cation $Na(OH_2)_n^+$ has a size that compares much more favorably with the anion than does the "naked" potassium ion. (2) The measured density (1.97 g/cm^3) is lower than those of polymeric potassium cyanocuprates (2.38 g/cm^3 for $KCu(CN)_2$ and 2.39 g/cm^3 for $KCu_2(CN)_3 \cdot H_2O$) and very close to the value found for the monomeric potassium tetracyanocuprate (2.02 g/cm^3). (3) For the CN:Cu ratio lower than 3, the solubility of the sodium cyanocuprates in water (where the ions are monomeric) is higher than for the potassium salts.[7] (4) The mononuclear planar tricyanocuprate ion $Cu(CN)_3^{2-}$ exists in solution as well as in the solid compound $Na_2Cu(CN)_3 \cdot 3H_2O$.[8]

Unfortunately our purpose was not successful and we found a new polymeric structure which we will describe herein.

Experimental Section

Preparation. Copper cyanide (2.25 g, 25 mmol) was dissolved in an aqueous solution (15 ml) of sodium cyanide (1.95 g, 40 mmol). After one night of cooling, a precipitation of needles occurred. The